Presynaptic MAST kinase controls opposing postsynaptic responses to convey stimulus valence in *Caenorhabditis elegans*

Shunji Nakano[a,b], Muneki Ikeda[b], Yuki Tsukada[a,b], Xianfeng Fei[c], Takamasa Suzuki[d], Yusuke Niino[e], Rhea Ahluwalia[b], Ayana Sano[b], Rumi Kondo[b], Kunio Ihara[f], Atsushi Miyawaki[e,g], Koichi Hashimoto[h], Tetsuya Higashiyama[b,i], and Ikue Mori[a,b,1]

[a]Neuroscience Institute, Graduate School of Science, Nagoya University, Nagoya, Aichi 464-8602, Japan; [b]Division of Biological Science, Graduate School of Science, Nagoya University, Nagoya, Aichi 464-8602, Japan; [c]Faculty of Science and Technology, Tohoku Bunka Gakuen University, Sendai, Miyagi 981-0943, Japan; [d]Department of Biological Chemistry, College of Bioscience and Biotechnology, Chubu University, Kasugai, Aichi 487-8501, Japan; [e]Laboratory for Cell Function and Dynamics, RIKEN Center for Brain Science, Wako-City, Saitama 351-0198, Japan; [f]Center for Gene Research, Nagoya University, Nagoya, Aichi 464-8602, Japan; [g]Biotechnological Optics Research Team, RIKEN Center for Advanced Photonics, Wako-City, Saitama 351-0198, Japan; [h]Graduate School of Information Sciences, Tohoku University, Sendai, Miyagi 980-8579, Japan; and [i]Institute of Transformative Bio-Molecules, Nagoya University, Nagoya, Aichi 464-8601, Japan

Edited by Paul W. Sternberg, California Institute of Technology, Pasadena, CA, and approved December 12, 2019 (received for review May 31, 2019)

Presynaptic plasticity is known to modulate the strength of synaptic transmission. However, it remains unknown whether regulation in presynaptic neurons can evoke excitatory and inhibitory postsynaptic responses. We report here that the *Caenorhabditis elegans* homologs of MAST kinase, Stomatin, and Diacylglycerol kinase act in a thermosensory neuron to elicit in its postsynaptic neuron an excitatory or inhibitory response that correlates with the valence of thermal stimuli. By monitoring neural activity of the valence-coding interneuron in freely behaving animals, we show that the alteration between excitatory and inhibitory responses of the interneuron is mediated by controlling the balance of two opposing signals released from the presynaptic neuron. These alternative transmissions further generate opposing behavioral outputs necessary for the navigation on thermal gradients. Our findings suggest that valence-encoding interneuronal activity is determined by a presynaptic mechanism whereby MAST kinase, Stomatin, and Diacylglycerol kinase influence presynaptic outputs.

C. elegans | thermotaxis | MAST kinase | Stomatin | Diacylglycerol kinase

Sensory stimuli that predict the valence of reward or punishment are major drivers of animal behaviors. For example, odors associated with predators are detrimental to the animals and elicit fear responses (1), while smells predicting the presence of food or potential mates evoke different behaviors such as feeding (2) or mating (3). Extracting the valence information of sensory stimulus—whether the stimulus is attractive or aversive—and manifesting appropriate behavioral responses are the most vital function of the nervous system. Deciphering the molecular and circuit mechanisms underlying the valence coding of sensory information is thus fundamental to understand the principles of how animal behaviors emerge from the nervous system.

The valences of innate odor responses are guided by intrinsic property of the responding neurons, in which neurons expressing specific odorant receptors are hardwired in a neural circuit that elicits attractive or aversive behavior (4, 5). A similar labeled-line circuit operation was also demonstrated for encoding and responding to tastes such as sweet and bitter (6, 7), wherein cells expressing specific taste receptors are embedded in a specialized neural circuit that promotes or inhibits feeding behaviors.

Contrary to these developmentally programmed, stereotyped behaviors, the valence associated with certain sensory stimuli can vary depending on the past experience, the current environmental context, and the stimulus intensity (8). For example, olfactory preferences to the same odorants can differ depending on the odorant concentration (9). Several studies suggested a common feature of neural mechanism underlying the change in these odorant valences, wherein different concentrations of the same odorants recruit distinct sets of olfactory neurons and consequently change the perception of the same odorants (10–12). In addition, recent studies proposed an alternative strategy, wherein a single population of neurons responds to appetitive or aversive stimuli and represents the positive or negative valence of the stimuli by increasing or decreasing neuronal activity (13, 14). Specifically, CRF (corticotropin-releasing factor)-releasing neurons in the paraventricular nucleus of the hypothalamus are activated by aversive stimuli and inhibited by appetitive stimuli (14). Likewise, in *Caenorhabditis elegans*, experience-dependent modulation enables a single set of interneurons to elicit opposing responses to carbon dioxide, which can be either attractive or aversive, depending on prior experience (13). Thus, these observations indicate a previously unrecognized mechanism of valence coding for even a single modality of stimulus, in which the opposing activity in a single population of neurons can be modulated by prior experience

Significance

Animals need to quickly extract the valence information of sensory stimulus and assess whether the stimulus is attractive or aversive. Deciphering the molecular and circuit mechanisms that determine the stimulus valence is fundamental to understand how the nervous system generates the animal behaviors. Here we report that the AFD thermosensory neurons of *C. elegans* evoke in its postsynaptic AIY interneurons opposing neuronal responses that correlate with the valence of thermal stimuli. The *C. elegans* homologs of MAST kinase, Stomatin, and Diacylglycerol kinase function in AFD and regulate the opposing AIY responses. Our results further suggest that the alteration between excitatory and inhibitory AIY responses is mediated by controlling the balance of two opposing signals released from the AFD neurons.

Author contributions: S.N. and I.M. designed research; S.N., T.S., R.A., A.S., R.K., K.I., and T.H. performed research; M.I., Y.T., X.F., Y.N., A.M., and K.H. contributed new reagents/analytic tools; S.N. analyzed data; and S.N. and I.M. wrote the paper.

The authors declare no competing interest.

This article is a PNAS Direct Submission.

Data deposition: The sequence of YCX1.6 reported in this paper has been deposited to DNA Data Bank of Japan (DDBJ)/European Molecular Biology Laboratory (EMBL)/GenBank (accession no. LC498642).

[1]To whom correspondence may be addressed. Email: m46920a@nucc.cc.nagoya-u.ac.jp.

This article contains supporting information online at https://www.pnas.org/lookup/suppl/doi:10.1073/pnas.1909240117/-/DCSupplemental.

First published January 7, 2020.

and environment to represent stimulus valence. However, little is known about the molecular mechanism and circuit logics for such modulation of valence-coding activity.

The compact nervous system of *C. elegans* consisting of only 302 neurons provides an excellent opportunity to explore these questions (15). *C. elegans* exhibits thermotaxis (TTX) behavior (16), in which the valence of thermal information varies depending on the past experience, current temperature environment, and feeding states. Specifically, the temperature preference of *C. elegans* is plastic and determined by the cultivation temperature, in which animals that are cultivated at a constant temperature with food migrate toward that cultivation temperature on a thermal gradient without food (16). When animals were placed at the temperature below the cultivation temperature, they migrate up the thermal gradient, while above the cultivation temperature they move down the gradient, indicating that the valence associated with thermal stimuli alternates in opposing manners depending on the current temperature.

Previous studies identified neurons involved in TTX (17–19). Of those neurons, the AFD thermosensory neurons are essential for TTX and are required for migrating up and down the thermal gradient to reach the cultivation temperature (18, 20). Calcium imaging analyses revealed that the AFD neuron displayed increases in calcium concentration upon warming phases of a temperature ramp both below and above the cultivation temperature (21–27). However, it remains to be determined how the AFD neuronal activities with similar calcium dynamics below and above the cultivation temperature are transformed to encode appropriate valence of temperature information and the consequent manifestation of opposing behavioral regulations.

Here we report that the AFD neuron evokes opposing neuronal responses in its postsynaptic partner AIY interneuron below or above the cultivation temperature: the activation of AFD neuron stimulates the AIY neuron below the cultivation temperature, while it inhibits AIY above that temperature. We identified molecular components important for this process and showed that this alteration of the AFD–AIY communication is regulated by presynaptic actions of the *C. elegans* homologs of MAST (Microtubule-Associated Serine-Threonine) kinase (28), Stomatin (29), and Diacylglycerol kinase (30, 31). Our results further suggest that the alteration of the AFD–AIY synaptic transmission is mediated by the balance of two opposing signals released from the AFD neuron, an excitatory peptidergic signaling and an inhibitory glutamatergic signaling. A high-throughput behavioral analysis suggested that MAST kinase, Stomatin, and Diacylglycerol kinase regulate opposing behavioral biases in the steering direction of animal locomotion to warmer or colder side of the temperature gradient, thereby driving the animals toward the cultivation temperature. Our results suggest that the valence-coding neuronal activity is regulated by presynaptic mechanism whereby the evolutionarily conserved MAST kinase, Stomatin, and Diacylglycerol kinase control the presynaptic release of opposing signaling molecules.

Results

***kin-4*, *mec-2*, and *dgk-1* Regulate the *C. elegans* TTX Behavior.** To elucidate the molecular and neural mechanisms underlying the valence coding of thermal stimuli during *C. elegans* TTX behavior, we conducted forward genetic screens and sought mutants that displayed abnormal TTX behavior. We found that mutations in three genes, *kin-4*, *dgk-1*, and *mec-2*, affected this behavior (Fig. 1). While the wild-type animals that had been cultivated at 20 °C preferred to stay around the cultivation temperature, loss-of-function mutants of *kin-4*, which encodes the *C. elegans* ortholog of the mammalian MAST kinase, displayed a cryophilic phenotype and migrated toward a colder temperature region than the wild-type animals (Fig. 1*B* and *SI Appendix*, Fig. S1*A*). This defect was rescued by introduction of a *kin-4* genomic clone (Fig. 1*C*), indicating that *kin-4* is required for TTX. Animals carrying mutations in the gene *dgk-1*, which encodes a homolog of Diacylglycerol kinase θ (30, 31), also preferred to migrate toward a colder temperature region (32) (Fig. 1*B* and *SI Appendix*, Fig. S1*A*). The cryophilic phenotype of *dgk-1(nj274)* mutants was rescued by introduction of a *dgk-1* genomic clone (*SI Appendix*, Fig. S1*B*), indicating that *dgk-1* is required for TTX. We also isolated a mutation in *mec-2*, which encodes a *C. elegans* homolog of Stomatin (29). *mec-2(nj89)* animals harbored a mutation that is predicted to alter the glutamic acid 270 to a lysine (*E270K*; *SI Appendix*, Fig. S1*A*) and displayed a thermophilic phenotype (Fig. 1*B*). Introduction of a mutant *mec-2(E270K)* clone into the wild-type animals phenocopied *mec-2(nj89)* mutants, while introduction of a wild-type *mec-2* clone into *mec-2(nj89)* mutants did not rescue the thermophilic defect (Fig. 1*D*). We also generated a null allele of *mec-2(nj251Δ)* (*SI Appendix*, Fig. S1*A*) and found that *mec-2* null mutants were grossly normal in TTX (*SI Appendix*, Fig. S1*C*), suggesting that some of the nine additional Stomatin genes encoded by the *C. elegans* genome could compensate the deficit of *mec-2*. These results indicate that *mec-2(nj89)* is a gain-of-function mutation and causes a thermophilic phenotype. To address the nature of the gain of function, we injected into the wild-type animals a wild-type genomic *mec-2* transgene at different concentrations and observed that introduction of the *mec-2(+)* transgene at a higher dose conferred a thermophilic phenotype (*SI Appendix*, Fig. S1*D*). These results indicate that the gain of the wild-type activity of *mec-2* can cause a thermophilic phenotype and suggest that *mec-2(nj89gf)* is likely a hypermorphic or altered-function mutation.

To address genetic interactions among these genes, we analyzed TTX behaviors of double mutants. Animals carrying mutations in both *kin-4* and *mec-2* showed a thermophilic phenotype similar to that of *mec-2* single mutants (Fig. 1*E*), suggesting that *mec-2* acts downstream of or in parallel to *kin-4*. Similarly, *dgk-1* mutations partially suppressed the thermophilic phenotype conferred by *mec-2(nj89gf)* mutation (Fig. 1*F*), suggesting that *dgk-1* acts downstream of or in parallel to *mec-2*. We hereafter focused on *kin-4(tm1049Δ)*, *mec-2(nj89gf)*, and *dgk-1(nj274Δ)* mutants for further analyses.

***kin-4*, *mec-2*, and *dgk-1* Function in the AFD Thermosensory Neuron to Regulate TTX.** To ask where *kin-4* and *mec-2* are expressed, we conducted expression analysis. We generated a functional *kin-4::gfp* translational transgene capable of rescuing the cryophilic phenotype of *kin-4* mutants (*SI Appendix*, Fig. S2*A*). This transgene was broadly expressed in the nervous system, and its expression was observed in neurons previously shown to be involved in TTX (17, 18, 33), including the AFD and AWC thermosensory neurons and the AIY and RIA interneurons (Fig. 2 *A* and *B* and *SI Appendix*, Fig. S2*B*). We also assessed expression of *mec-2* and found that a *Pmec-2c::gfp* reporter was expressed in AFD and AWC (Fig. 2*B*). Consistent with a previous report (29), we observed expression in mechanosensory neurons when *gfp* was fused to a promoter for another *mec-2* isoform, *mec-2a* (*SI Appendix*, Fig. S2*C*). A previous study also showed that *dgk-1* was ubiquitously expressed in the nervous system (31). These results suggest that *kin-4*, *mec-2*, and *dgk-1* are expressed in neurons known to be involved in regulation of TTX, including the AFD and AWC thermosensory neurons.

To identify the neuron(s) in which *kin-4*, *mec-2*, and *dgk-1* act to regulate TTX, we attempted to express each of these genes in single neurons and assessed their effects on the TTX behavior. Expression of a *kin-4* cDNA in AFD rescued the cryophilic phenotype of *kin-4* mutants, whereas expression in AWC, AIY, AIZ, or RIA did not (Fig. 2*C*), indicating that *kin-4* functions in AFD to regulate TTX. When mutant *mec-2(E270K)* was expressed in AFD, it phenocopied *mec-2(nj89gf)* mutants, while expression in AWC did not (Fig. 2*D*). Expression of a *dgk-1*

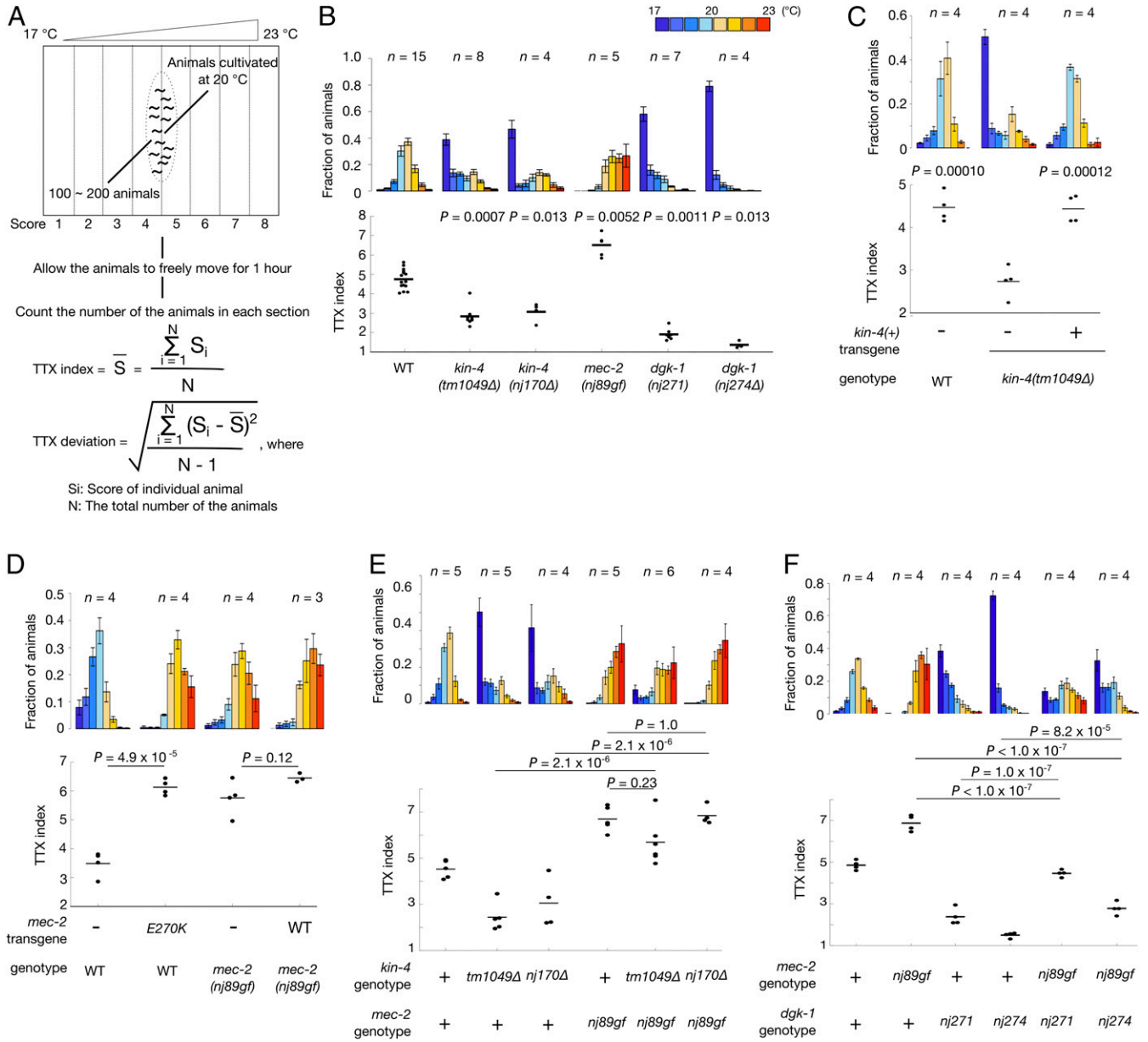

Fig. 1. *kin-4*, *mec-2*, and *dgk-1* regulate the *C. elegans* TTX behavior. (*A*) Procedure of TTX assay is shown. Animals were cultivated at 20 °C and were placed on the center of a thermal gradient ranging from 17 °C to 23 °C. Each assay typically contains 100 to 200 animals. Distribution of the animals in each section of the assay plate was determined. We also use TTX index and TTX deviation to quantify the behavior (71). The formula of TTX index and TTX deviation are shown. (*B–F*) TTX behavior of the wild-type, *kin-4*, *mec-2*, and *dgk-1* mutant animals. Distributions of the animals in each section of the assay plate (*Top*) are shown as means ± SEM. TTX indices (*Bottom*) are shown as dots. Lines indicate the means. *n* represents the number of independent experiments. *P* values were determined by Kruskal–Wallis test with Steel method for comparison to the wild-type animals in *B*, one-way ANOVA with Dunnett's test for comparison to *kin-4(tm1049Δ)* mutants in *C*, two-tailed Student's *t* tests in *D*, and one-way ANOVA with Tukey–Kramer test in *E* and *F*.

cDNA in AFD but not in AWC partially rescued the cryophilic phenotype of *dgk-1* mutants, but the *dgk-1* mutants expressing *dgk-1* only in AFD distributed rather evenly on the temperature gradient, as evidenced by their high value of TTX deviation (Fig. 2*E*). We observed that simultaneous expression of *dgk-1* in both AFD and AWC fully rescued the *dgk-1* mutant phenotype. These results indicate that *kin-4*, *mec-2*, and *dgk-1* function in AFD to regulate TTX.

***kin-4*, *mec-2*, and *dgk-1* Act Downstream of Calcium Influx in AFD.** To assess whether *kin-4*, *mec-2*, and *dgk-1* regulate temperature-evoked activity of the AFD thermosensory neuron, we conducted calcium imaging of AFD. We immobilized animals expressing the GCaMP3 calcium indicator in AFD and subjected the animals to a warming stimulus. Consistent with previous reports (21–27), we observed that the AFD neuron showed increases in calcium concentration upon warming stimuli both below and above the cultivation temperature (*SI Appendix*, Fig. S3 *A* and *B*), and this response required three guanylate cyclase genes, *gcy-8*, *gcy-18*, and *gcy-23*, exclusively expressed in the AFD neurons (23, 25, 34) (*SI Appendix*, Fig. S3*B*). The temperature-evoked calcium responses of AFD in *kin-4*, *mec-2*, and *dgk-1* mutants were almost indistinguishable from that of the wild-type animals (*SI Appendix*, Fig. S3 *B–D*). These results suggest that *kin-4*, *mec-2*, and *dgk-1* regulate a process downstream of the calcium influx in AFD.

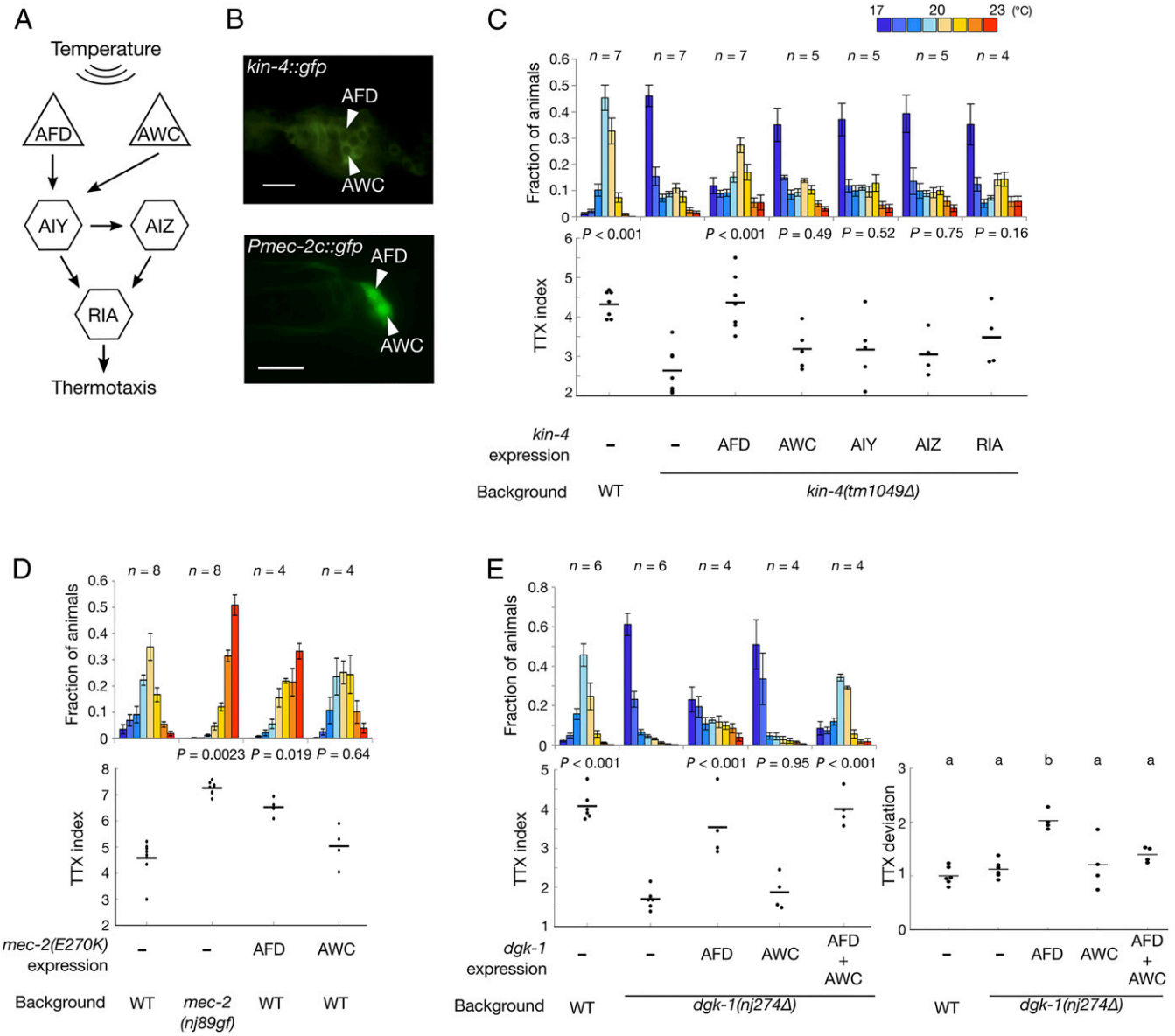

Fig. 2. *kin-4*, *mec-2*, and *dgk-1* function in the AFD thermosensory neurons to regulate TTX. (*A*) Neural circuit involved in TTX. Arrows indicate chemical synapses. Triangles and hexagons represent sensory and interneurons, respectively. (*B*) Expression analyses of *kin-4::gfp* (*Top*) and *Pmec-2c::gfp* (*Bottom*). Head regions of animals are shown. The arrowheads indicate the AFD and AWC sensory neurons. (Scale bars, 10 μm.) (*C*–*E*) TTX behaviors of animals in which *kin-4*, *mec-2(E270K)*, or *dgk-1* cDNA was specifically expressed in AFD and other neurons. Animals were cultivated at 20 °C. Distributions of animals in each section of the assay plates are shown as means ± SEM. TTX indices and TTX deviations are shown as dots, and the lines indicate means. *n* indicates the number of the independent experiments. Animals were cultivated at 20 °C. For comparisons of TTX indices, *P* values were determined by one-way ANOVA with Dunnett's test for multiple comparison to *kin-4(tm1049Δ)* in *C* or *dgk-1(nj274Δ)* in *E*. Kruskal–Wallis test with Steel method was used for comparison to the wild-type animals in *D*. Tukey–Kramer test was performed for comparison of TTX deviations in *E*, and different letters denote statistically significant groups.

Valence of Thermal Information Is Encoded by Opposing AIY Response. To ask whether *kin-4*, *mec-2*, and *dgk-1* regulate the activity of the AIY interneuron, the sole chemical postsynaptic partner of AFD (15), we monitored calcium dynamics of both AFD and AIY. We generated the animals expressing the YCX1.6 yellow cameleon ratiometric calcium indicator in both AFD and AIY and subjected them to warming stimuli while they were freely moving under the microscope with an automated tracking system (Fig. 3*A*). We first subjected animals to a warming stimulus below the cultivation temperature, in which the temperature was increasing toward the cultivation temperature (Fig. 3*B*). When the wild-type animals were exposed to this warming stimulus, the AFD neuron showed an increase in calcium concentration with its peak around 17 to 19 s after the thermal stimulus was applied, and this trend of the AFD responses was evident in almost all of the recording (Fig. 3*C*). By contrast, the responses of the AIY neuron were probabilistic, with some responses appearing to be excitatory while the others were inhibitory (Fig. 3*C*). We quantified the area under the curve of the AIY responses to categorize the AIY response and found that more than half of the AIY responses were categorized as excitatory under this condition (*SI Appendix*, Fig. S4*A*). When we subjected the animals to a warming stimulus above the cultivation temperature, where the temperature was increasing away from the cultivation temperature (Fig. 3*E*), the AIY neuron primarily showed a decrease in calcium concentration, despite the consistent trend of increase in the AFD calcium level (Fig. 3*F* and

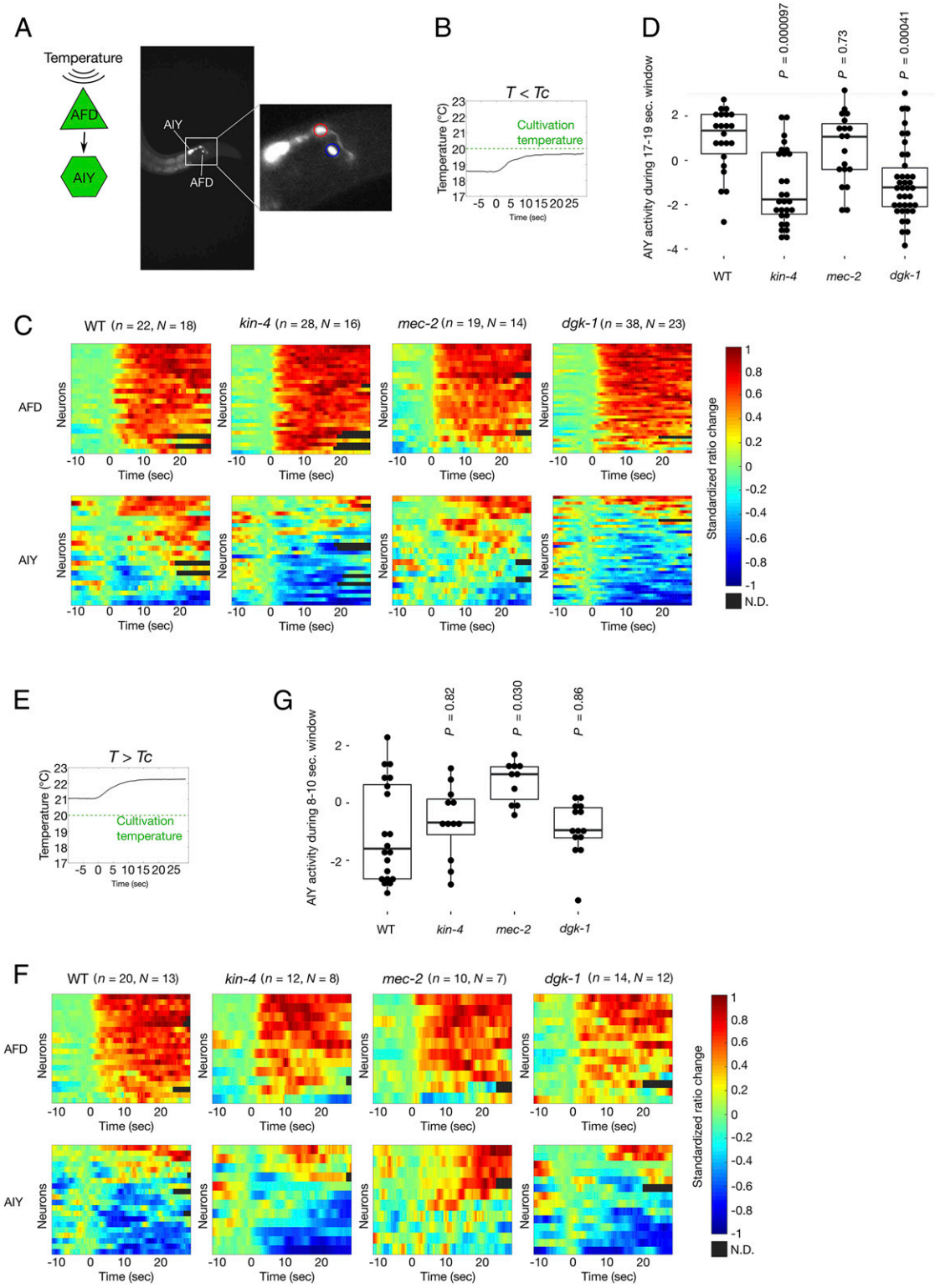

Fig. 3. The opposing AIY response encodes stimulus valence and is regulated by *kin-4, mec-2*, and *dgk-1*. Calcium imaging of AFD and AIY neurons in freely moving animals. (*A*) Neurons imaged are shown (*Left*). A representative image of the tracking experiment (YFP channel) is shown (*Middle*). Cell bodies of AFD and AIY are indicated. A magnified view of the head region of the animal is shown (*Right*). Regions from which AFD and AIY fluorescence signals were measured are indicated by blue and red circles, respectively. (*B–D*) Calcium imaging below the cultivation temperature. (*E–G*) Calcium imaging above the cultivation temperature. (*B* and *E*) The temperature program used. (*C* and *F*) Heat maps representing standardized ratio changes of AFD (*Top*) and AIY (*Bottom*) calcium dynamics. Each row indicates the response observed each recording. Time 0 corresponds to the onset of the warming stimulus. Standardized ratio change is represented in the color bar to the right. *n* indicates the number of trials. *N* indicates the number of animals observed. (*D* and *G*) Comparisons of AIY activities during 17 to 19 s (*D*) or 8 to 10 s (*G*) after the thermal stimulus was applied. The area under the curve of AIY standardized ratio change was calculated for each animal. Individual data points are shown as dots. Boxes display the first and third quartiles, lines inside the boxes are the medians, and the whiskers extend to 1.5-time interquartile range from the box. *P* values were determined by Kruskal–Wallis test with Steel method to compare to the wild-type animals.

SI Appendix, Fig. S4*A*). We also conducted cross-correlation analysis of AFD and AIY activity (*SI Appendix*, Fig. S4*B*) and observed that the median value of AIY–AFD cross correlation peaks at the lag of 5.5 s for excitatory responses below the cultivation temperature, suggesting that the excitatory AIY response followed the AFD response, whereas the median value for inhibitory responses above the cultivation temperature peaks at −0.5 s. Together, these results indicate that the probabilistic nature of opposing AIY responses correlates with the valences of thermal stimuli, with temperature increase toward the cultivation temperature evoking excitatory response and temperature increase away from the cultivation temperature inhibitory response.

A recent study reported that the difference in the AIY calcium responses below or above the cultivation temperature was represented by a difference in the fraction of animals in which AIY showed an increase in calcium concentration upon warming (35). Two major differences in the experimental conditions might account for the differences in the observed AIY responses: one is that the different calcium indicators were used (GCaMP3 in the previous study and YCX1.6 in this study), and the other is whether the animals were immobilized or allowed to freely move. To address these possibilities, we used the same wild-type strain expressing the YCX1.6 calcium indicator and conducted calcium imaging under immobilized conditions (*SI Appendix*, Fig. S4 *C* and *D*). When the animals were subjected to warming stimuli below or above the cultivation temperature, the majority of the AIY responses appeared to be excitatory (*SI Appendix*, Fig. S4 *A*, *C*, and *D*), and we did not observe increases in the fraction of inhibitory responses above the cultivation temperature. These results suggest that whether animals are immobilized or not could influence the AIY activity. The precise reasons that caused the difference between immobilized and freely moving condition remain to be determined. A previous study showed that impeded motor execution by either pharmacological or physical method leads to prolongation of high-activity phases of reversal-promoting neurons (36). Since the AIY activity is low during reversal phase (37, 38), we speculate that immobilization of animals by certain methods, including ours, induces prolonged reversal state in the nervous system and reduces the AIY activity, which might mask the effect of inhibitory input from the temperature stimulus. We also note that the immobilization methods used in this study and the previous study (35) are different (beads in this study and chemical anesthetic in the previous study).

***kin-4*, *mec-2*, and *dgk-1* Regulate Opposing AIY Responses.** We next examined the AIY responses in *kin-4*, *dgk-1*, and *mec-2* mutants under freely moving conditions. The AIY neuron in *kin-4* mutants predominantly exhibited a decrease in calcium concentration even below the cultivation temperature, the condition in which the wild-type AIY neuron would primarily respond by increasing its calcium level (Fig. 3 *C* and *D* and *SI Appendix*, Fig. S5). Consistent with the calcium imaging analysis of AFD in immobilized animals (*SI Appendix*, Fig. S3), the AFD neuron of *kin-4* mutants showed increases in calcium concentration both below and above the cultivation temperature (Fig. 3 *C* and *F*). The defect in the AIY response of *kin-4* mutants was partially rescued by expression of a *kin-4* cDNA solely in the AFD neuron (*SI Appendix*, Fig. S6 *A*–*C*), indicating that the AIY calcium response is indeed modulated by its presynaptic partner AFD. A similar response profile was also observed in the cryophilic *dgk-1* mutants: the AIY calcium level dropped upon warming stimuli both below and above the cultivation temperature in most of the trials, while the AFD neuron responded to the warming stimuli by increasing the calcium concentration (Fig. 3 *C*, *D*, *F*, and *G* and *SI Appendix*, Fig. S5). This defect in the AIY response of *dgk-1* mutants was fully rescued when a *dgk-1* cDNA was expressed either only in AFD or simultaneously in AFD and AWC (*SI Appendix*, Fig. S6 *B* and *D*). Given that the TTX defect of *dgk-1* was fully rescued only when *dgk-1* was expressed simultaneously in AFD and AWC (Fig. 2*E*), these observations suggest that the function of *dgk-1* in AWC might be mediated through neurons other than AIY. We also observed that in the thermophilic *mec-2* mutants, the majority of their AIY responses did not show clear decreases in calcium concentration even above the cultivation temperature (Fig. 3 *F* and *G* and *SI Appendix*, Fig. S5). Similarly to the wild type, the AFD neurons in *mec-2* mutants showed increases in calcium concentration under both conditions tested (Fig. 3 *C* and *F*). This abnormality of the AIY response was recapitulated by expressing mutant *mec-2* cDNA only in AFD (*SI Appendix*, Fig. S6 *F* and *G*). These results indicate that the valence-coding AIY activity is regulated by *kin-4*, *mec-2*, and *dgk-1*. Given that expression of these genes only in AFD rescued or phenocopied the defect of the AIY response in the respective mutants, these results further suggest that presynaptic regulation is important for determining the valence-encoding activity of the AIY neuron.

Alteration of the AFD–AIY Synaptic Transmission Requires Components Essential for Neuropeptide and Glutamate Release. We next asked how the presynaptic regulation in AFD evokes opposing neuronal responses in the AIY postsynaptic neuron. Previous studies indicated that AFD employs two kinds of signaling molecules to communicate with AIY (33, 39): one is neuropeptide, and the other is glutamate. The peptidergic signaling was shown to be excitatory (39), whereas the glutamatergic input is inhibitory due to a glutamate-gated chloride channel acting on AIY (33). We hypothesized that the balance of these two opposing signals released from AFD might be modulated, thereby inducing an excitatory or inhibitory postsynaptic response. To test this possibility, we monitored the AIY calcium response in mutants for the gene *unc-31*, which encodes the *C. elegans* ortholog of calcium-dependent activator protein required for secretion of neuropeptides (40). The AIY neurons of *unc-31* mutants predominantly showed a decrease in the calcium concentration even below the cultivation temperature, while the AFD neuron showed increases in calcium concentration under both conditions tested (Fig. 4 *A*–*C* and *SI Appendix*, Fig. S5). This defect in the AIY response was partially rescued by expression of an *unc-31* cDNA only in AFD (*SI Appendix*, Fig. S7 *A*–*C*), indicating that the peptidergic signals from AFD is required for the opposing AIY response.

We also examined the AIY response in mutants for the *eat-4* gene, which encodes a *C. elegans* homolog of vesicular glutamate transporter required for transporting glutamate into synaptic vesicles (41). In *eat-4* mutants, the AIY neurons did not display primarily decreases in the calcium concentration above the cultivation temperature when compared to the wild-type animals (Fig. 4 *D*–*F* and *SI Appendix*, Fig. S5), and this defect was rescued by expression of *eat-4* only in the AFD neurons (*SI Appendix*, Fig. S7 *D*–*F*). Like in *unc-31* mutants, the AFD neurons in *eat-4* mutants showed increase in the calcium level under both conditions tested. We also noted that the AIY response in *eat-4* mutants below the cultivation temperature was reduced compared to the wild-type animals (Fig. 4 *B* and *C*). These results suggest that alteration of the positive and negative modes of the AFD–AIY communication requires the presynaptic control of the glutamatergic and peptidergic outputs.

***kin-4*, *mec-2*, and *dgk-1* Regulate Curving Bias During TTX.** To address how the alteration in the modes of the AFD–AIY communication contributes to the regulation of TTX behavior, we undertook multiworm tracking analysis (42). We classified the animal behavior into several behavioral components discernable during *C. elegans* locomotion, such as forward locomotion, omega turn, shallow turn, reversal, and reversal turn (43–47). Previous studies showed that the wild-type animals modulate the run durations such that the duration of run toward the cultivation temperature would be lengthened (20, 48–50). In addition,

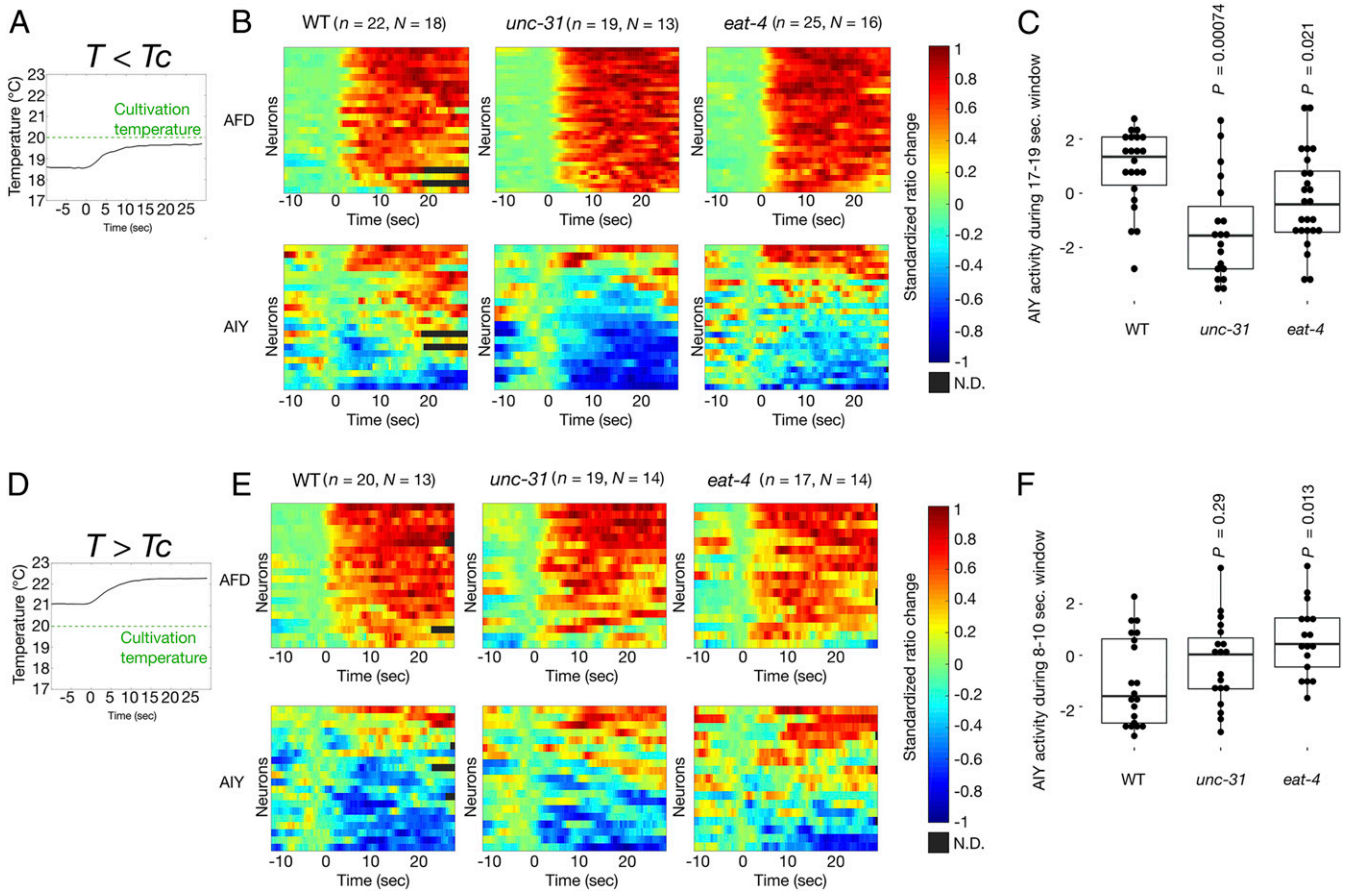

Fig. 4. Alteration of the AFD-AIY synaptic valence requires components essential for neuropeptide and glutamate release. (*A*–*C*) Calcium imaging below the cultivation temperature. (*D*–*F*) Calcium imaging above the cultivation temperature. (*A* and *D*) The temperature program used. (*B* and *E*) Heat maps representing standardized ratio changes of AFD (*Top*) and AIY (*Bottom*) calcium dynamics. Each row indicates the response observed each recording. Time 0 corresponds to the onset of the warming stimulus. Standardized ratio change is represented in the color bar to the right. *n* indicates the number of trials. *N* indicates the number of animals observed. (*C* and *F*) Comparisons of AIY activities during 17 to 19 s (*D*) or 8 to 10 s (*G*) after the thermal stimulus was applied. The area under the curve of AIY standardized ratio change was calculated for each animal. Individual data points are shown as dots. Boxes display the first and third quartiles, lines inside the boxes are the medians, and the whiskers extend to 1.5-time interquartile range from the box. *P* values were determined by Kruskal–Wallis test with Steel method to compare to the wild-type animals. Note that the wild-type data are identical to those shown in Fig. 3 and indicated here for comparison to *unc-31* and *eat-4* mutants.

C. elegans also controls steering during chemotaxis, in which the animals curve during forward locomotion toward higher concentration of attractants (46). We assessed whether the animals utilize both of these strategies under our condition of TTX assay and observed that the wild-type animals displayed a bias in the curve: the animals curve toward warmer temperature below the cultivation temperature and curve toward colder temperature above the cultivation temperature (Fig. 5 and *SI Appendix*, Fig. S8*A*, and see also ref. 43). In addition, consistent with the previous reports of regulation of run duration during TTX (20, 48–50), we observed that the wild-type animals exhibited a significant bias in the frequency of reversal turn. They showed higher reversal turn frequency when they migrate away from the cultivation temperature than when they migrate toward the cultivation temperature (*SI Appendix*, Fig. S8*B*, and see also ref. 43): below the cultivation temperature ($T < Tc$), reversal turn frequency was higher when migrating down the gradient ($\theta \geq 90°$) than migrating up the gradient ($\theta < 90°$), while above the cultivation temperature ($T > Tc$), the frequency was higher when migrating up the gradient than down the gradient. We did not observe such significant bias in the frequency of shallow turn, omega turn, or reversal (*SI Appendix*, Fig. S8).

We asked whether *kin-4*, *mec-2*, and *dgk-1* mutations affect regulation of these behavioral components and found that they displayed defects in curve that are in parallel with their TTX phenotypes. Both *kin-4* and *dgk-1* cryophilic mutants displayed abnormal curving bias toward colder temperature when migrating up the gradient below the cultivation temperature (Fig. 5). By contrast, thermophilic *mec-2* mutants showed curving bias toward warmer temperature when migrating up the gradient above the cultivation temperature. We also found that *kin-4* and *dgk-1* mutations affected the regulation of reversal turn. Below the cultivation temperature, the bias in the frequency of reversal turn that would drive the wild-type animals toward higher temperature was lost or reversed in *kin-4* or *dgk-1* mutants, respectively (*SI Appendix*, Fig. S8*B*). We did not observe changes in the bias of reversal turn frequency in *mec-2* mutants, although the frequencies of reversal turn were lower than those of the wild-type animals. In addition, we conducted similar analysis of *eat-4(ky5)* mutants and observed that they also affected bias in the curve and reversal turn (Fig. 5 and *SI Appendix*, Fig. S8*B*). These results indicate that *kin-4*, *mec-2*, and *dgk-1* regulate the curve during TTX and suggest that the alteration of the AFD–AIY synaptic transmission generates opposing curving biases that drive the animals toward the cultivation temperature.

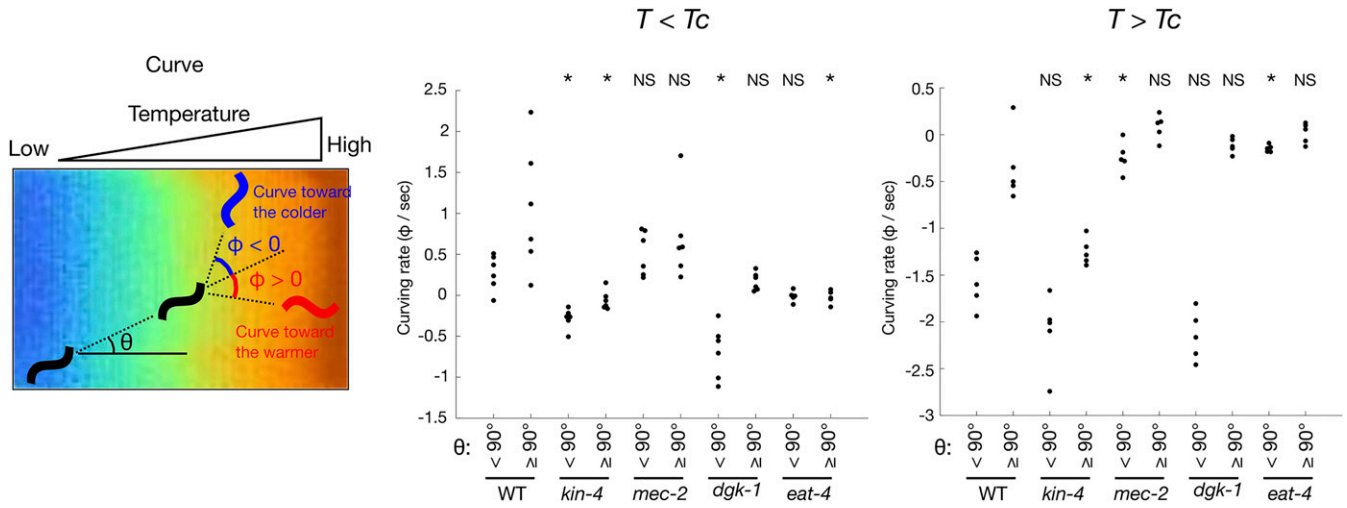

Fig. 5. *kin-4*, *mec-2*, and *dgk-1* regulate curving bias during TTX. Multiworm tracking analyses of curve. Schematics of curve is shown (*Left*). Animals were cultivated at 20 °C (*Tc*), and their behaviors within the temperature ranges from 17.0 °C to 20.0 °C (*Middle*; $T < Tc$) or from 20 °C to 23.0 °C (*Right*; $T > Tc$) were monitored. Curve is characterized by two angles ϕ and θ, where ϕ corresponds to the change in the moving direction during forward locomotion, and θ is the animal's previous moving direction relative to the vector pointing to the warm side of the temperature gradient. ϕ is given as a positive value if the angle change is directed toward the warmer side and a negative value if directed toward the colder side (*Left*). Dot plots of mean curving rate of animals migrating up the temperature gradient below (*Middle*) or above (*Right*) the cultivation temperature. The curving rates of all animals during the first 10 min of TTX assay were averaged and shown as dots. $*P < 0.05$, and *P* values were determined by Kruskal–Wallis test with Steel method for comparison to the wild-type animals. $n = 5$ to 6 recordings per condition.

Discussion

When animals encounter environmental stimuli, they need to quickly assess whether the stimuli are beneficial or detrimental. How the brain determines whether the valence of sensory information is attractive or aversive has been a fundamental question in neurobiology. Recent studies indicated that the opposing valences of sensory stimuli can be encoded by opposing activity of single population of neurons (13, 14, 51). In this study, we report the molecular components important for determining a valence-coding activity of a single class of interneuron and show that MAST kinase, Stomatin, and Diacylglycerol kinase control the activity of the AIY neuron that correlates with the valence of thermal stimuli. Our results also reveal a circuit principle of such valence coding, in which a single presynaptic neuron modulates its neuronal outputs and evokes an excitatory or inhibitory postsynaptic response.

Our results suggest that the mechanism of valence coding in thermal stimuli shares striking similarity to that of carbon dioxide in *C. elegans* (13, 51). *C. elegans* can display attraction or repulsion to CO_2, and this preference can be modulated by the prior experience of CO_2 concentration. Both CO_2 attraction and repulsion are mediated by a single sensory neuron BAG and a defined set of interneurons including AIY. A recent study showed that the AIY response to CO_2 stimulus can be either excitatory or inhibitory, depending on the prior experience of CO_2 (13). Thus, these results together with our observations suggest that bidirectional activity of a single set of interneurons could be a prevalent mechanism of valence coding for varieties of sensory stimuli in *C. elegans*. Further studies will be required to assess whether CO_2 circuit and thermosensory circuit share molecular mechanisms for eliciting the bidirectional interneuron activity.

We showed that *kin-4*, *mec-2*, and *dgk-1* regulate the curving bias during TTX behavior (Fig. 5). A previous study also showed that optogenetic manipulations of the AIY activity evoked biases in the curve: stimulation of AIY caused the animals to turn in the direction in which the head of the animal was bent at the time of the AIY excitation, while inhibition of AIY induced the animals to turn in the opposite direction (52). We also know from a previous report that the AFD neuron exhibits an increase in the calcium concentration when the head swings toward warmer temperatures on a thermal gradient (24). Given these observations, our results suggest that below the cultivation temperature, a warming stimulus activates both AFD and AIY, leading to a curve toward the warmer side of the temperature gradient, while above the cultivation temperature, a warming stimulus activates AFD, which in turn inhibits AIY, resulting in curving toward the colder side (*SI Appendix*, Fig. S9). Thus, the alteration of the AFD–AIY transmission mode would generate the curving bias that drives the animals toward the cultivation temperature.

Our results suggest that peptidergic signaling from AFD is required for the excitatory response of the AIY neuron, whereas glutamatergic signaling is required for the inhibitory response. This is consistent with our cross-correlation analysis of AIY–AFD responses, which suggested that the inhibitory AIY responses occur faster than the excitatory AIY responses (*SI Appendix*, Fig. S4*B*). However, our observation also suggested that the effects of these signaling pathways might not be strictly excitatory or inhibitory. For example, the excitatory response of the AIY neuron was attenuated in *eat-4* mutants (Fig. 4 *B* and *C*), suggesting that glutamate signaling might also be important for the excitatory response of the AIY neuron. Some of our observations also suggest that cells other than AFD could influence the AIY response upon temperature stimulus. Expression of *kin-4* and *unc-31* only in AFD partially restored the AIY responses but did not fully rescue the response to the wild-type level (*SI Appendix*, Figs. S6 *B* and *C* and S7 *B* and *C*), suggesting that *kin-4* and *unc-31* might also function in cells other than AFD to regulate the AIY response.

Recent investigation of the global brain dynamics in *C. elegans* revealed that most interneuron layers represent the motor states of the animals (36). Indeed, representation of the motor states is pervasive even in the first-layer interneurons that receive direct inputs from sensory neurons. The activity of the AIB interneuron, which is directly innervated by gustatory sensory neurons ASE and olfactory neurons AWC, is correlated with reversals (37), and the AIY neuron can represent multiple motor states (37, 38, 52). Because calcium dynamics within the AFD, ASE, and AWC neurons represent the respective sensory stimuli

(21, 22, 53–55), these observations suggest that transformation of sensory information into motor representation occurs early in the neural circuit and underlies between the sensory neurons and the first-layer interneurons.

Our results indicate that the initial step of information processing that transforms thermal information into stimulus valence occurs within the AFD sensory neuron and suggest that information processing for this transformation resides in cellular processes between calcium influx and neurotransmitter release. Our observations also suggest that this process of axonal computation is regulated by *kin-4*, *mec-2*, and *dgk-1*, although the interpretation of the involvement of *mec-2* has to be cautious, given the effect of *mec-2* on TTX was only observed in the *nj89* gain-of-function mutants. Previous studies established that MEC-2/Stomatin regulates the activity of amiloride-sensitive sodium channel (56). It remains to be determined whether KIN-4, MEC-2, and DGK-1 are involved in the regulation of such ion channels to impact on the release of neurotransmitter from AFD. Utilization of the recently developed optical sensors for neurotransmitters (57–60) would unveil the dynamics of axonal computations and help dissect the mechanisms by which *kin-4*, *mec-2*, and *dgk-1* regulate the release of either or both of glutamate and neuropeptide from the AFD neuron.

Neurons expressing multiple neurotransmitters are present in virtually all animal species (61, 62). A number of studies reported cotransmission of diverse combinations of multiple transmitters, including glutamate/GABA (63), dopamine/GABA (64), dopamine/glutamate (65), and different neuropeptides (66). Cotransmission of multiple transmitters from single neurons can influence the same target neurons (convergent actions) or different targets (divergent actions), thereby providing additional flexibility to the circuit functions and behaviors. In *Aplysia* neuromuscular junction, multiple cotransmitted peptides exert antagonistic actions, with one peptide promoting muscle contraction and the other increasing relaxation rate (67, 68). In this case, multiple transmitters are copackaged and coreleased in a fixed ratio. The apparently antagonistic actions of multiple transmitters likely facilitate rhythmic muscle contraction, thereby providing temporal flexibility in the circuit function (67, 68).

Our results suggest that by altering the balance of multiple transmitters with opposing actions, a single presynaptic neuron can evoke excitatory and inhibitory postsynaptic responses, convey the valence information of sensory stimulus to the circuit, and induce an appropriate behavior. We speculate that such mechanism of presynaptic control might function in other systems and be particularly effective in assigning the stimulus valence over a range of stimulus intensity. Thus, presynaptic control of multitransmitter release could be a fundamental mechanism of generating plasticity without extensive structural modification on the defined neural circuitry, thereby extending the computational repertoire employed by the nervous system.

Materials and Methods

All data, associated protocols, code, and materials used in this study will be available upon request to the corresponding author. *C. elegans* strains used in this study, TTX behavioral assays, forward genetic screens, expression analysis, calcium imaging of AFD neurons from immobilized animals, multiworm tracking analysis, and statistics are described in *SI Appendix, SI Methods*.

Generation of a New Calcium Probe YCX1.6. We used a newly developed calcium probe, YCX1.6, for simultaneous imaging of AFD and AIY in freely moving or immobilized animals. YCX1.6 was generated by incorporating four mutations within CaM-M13 domain of YC2.60 (69). YCX1.6 is a high-affinity variant of YC (yellow cameleon) X, which is characterized by expanded dynamic range (70). The apparent dissociation constant for Ca^{2+} and the Hill coefficient were calculated to be 120 nM and 1.2, respectively.

Simultaneous Calcium Imaging of AFD and AIY in Freely Moving or Immobilized Animals. We generated animals expressing the YCX1.6 probe in AFD and AIY. YCX1.6 in AFD was localized to the nucleus to separate the fluorescence signals from these neurons. For recording of freely moving animals, animals were cultivated at 20 °C and placed on a 2 to 2.5% agarose pad on a cover glass. The sample was covered by another cover glass and was placed onto a transparent temperature-controlled device (TOKAI HIT Co. Ltd.). This device was installed onto a motorized stage (HawkVision Inc.) that keeps the target image of animals in the field of view. Controlling the stage movement was achieved by real-time analysis of transmitted infrared light images. The animals were allowed to freely move under the microscope and were subjected to warming stimulus. We attempted to record each animal twice, but our tracking system sometimes failed to keep tracking the animals during the temperature stimulus given to the animal. We limited the number of the times that single animals exposed to the temperature program and avoided exposure to the temperature program for three times or more. For evaluation of the variance of the two recordings from identical animals, please see *SI Appendix*, Fig. S10. The recordings that persisted longer than 30 s were used for analysis. The fluorescence images were captured twice a second and split into YFP and CFP channels by W-VIEW GEMINI (Hamamatsu photonics K.K.). The YFP and CFP fluorescence intensities were obtained from the cell body of AFD and an axonal region of AIY (26). The fluorescent images were analyzed by a custom-written program in MATLAB with manual inspection of region of interest of AFD and AIY in every frame, and the fluorescent intensities of YFP and CFP were determined. Because of this intensive labor required for the image analysis, we did not perform the imaging of mutants or transgenic animals in parallel to the wild-type control. After determining the YFP and CFP intensity, we eliminated from the analysis the trials in which the temperature program failed to activate AFD. For this purpose, we applied a low-pass filter to the YFP/CFP ratio with the cutoff frequency at 0.05 Hz, and the resulting ratio data were used to calculate the ratio change. We eliminated from the analysis the trails in which the maximum ratio changes were smaller than 0.25 for recordings below the cultivation temperature or 0.22 for above the cultivation temperature. These threshold values were determined from experiments in which the temperature was kept constant. For the remainder of the trials, the ratio of fluorescence intensities (YFP/CFP) was used to calculate the standardized ratio change of AFD and AIY, which was defined as (ratio – minimum ratio)/(maximum ratio – minimum ratio). The baseline standardized ratio, which was the mean of the standardized ratio values of 5 consecutive frames immediately before the onset of warming stimulus, was subtracted from the standardized ratio change of each frame. For frames in which images were not available due to a failure of tracking the animals during recording, no value was assigned to these frames, and the data were represented as N.D. To categorize the AIY response, we used the MATLAB cumtrapz function and calculated the area under the curve of the AIY standardized ratio change for the entire time window after the temperature stimulus was applied. The AIY response was categorized as excitatory if the calculated area was positive and as inhibitory if the area was negative. For cross-correlation analysis of AIY and AFD activity, the mean AFD (AIY) standardized ratio change of each recording was subtracted from the time series of the AFD (AIY) standardized ratio change of that recording. The resulting AFD and AIY series of single recording were used for cross-correlation analysis. Cross-correlation was calculated by the MATLAB function xcorr with the scale option "unbiased" for normalization. For comparison of the AIY activity across strains, we calculated the area under the curve of the AIY standardized standardized ratio change between 17 and 19 s ($T < Tc$) or 8 and 10 s ($T > Tc$) after the onset of temperature ramp. These time windows correspond to the time at which the mean of AFD standardized ratio change in the wild-type animals reached to the maximum value ($T < Tc$) or first exceeded 0.5 ($T > Tc$).

For recording of immobilized animals, the animals were immobilized by placing on a 5 to 10% agarose pad with polystyrene beads. The fluorescence intensities of YFP and CFP were analyzed by the MetaMorph software. The calculation of standardized ratio change and the categorization of the AIY response were determined in the same way as described for the recording of freely moving animals above.

ACKNOWLEDGMENTS. We thank Y. Kohara and K. G. Miller for cDNAs; S. Mitani at National BioResouce for strains; K. Noma for comments on this manuscript; H. Matsuyama for discussion; and K. Ikegami, Y. Murakami, J. Okada, T. Sakaki, K. Sawayama, and F. Takeshige for technical assistance. M.I. was supported by Grant-in-Aid for Scientific Research 16J05770. This work was supported by Japan Society for the Promotion of Science (JSPS) Grant-in-Aid for Scientific Research Grant Numbers 17K07499 (to S.N.), 18H05123 (to S.N.), 26560549 (to Y.T.), 16H06536 (to K.H.), 18H04693 (to I.M.), 16H01272 (to I.M.), and 16H02516 (to I.M.); The Exploratory Research for Advanced Technology (ERATO) project (JPMJER1004 to T.H.) from Japan Science and Technology (JST) Agency; and the Brain Mapping by Integrated Neurotechnologies for Disease Studies (Brain/MINDS) JP19dm0207001 (to A.M.).

1. H. Zangrossi, Jr, S. E. File, Behavioral consequences in animal tests of anxiety and exploration of exposure to cat odor. *Brain Res. Bull.* **29**, 381–388 (1992).
2. L. M. Terry, I. B. Johanson, Olfactory influences on the ingestive behavior of infant rats. *Dev. Psychobiol.* **20**, 313–331 (1987).
3. R. E. Johnston, Effects of female odors on the sexual behavior of male hamsters. *Behav. Neural Biol.* **46**, 168–188 (1986).
4. S. Min, M. Ai, S. A. Shin, G. S. B. Suh, Dedicated olfactory neurons mediating attraction behavior to ammonia and amines in *Drosophila*. *Proc. Natl. Acad. Sci. U.S.A.* **110**, E1321–E1329 (2013).
5. K. Kobayakawa *et al*., Innate versus learned odour processing in the mouse olfactory bulb. *Nature* **450**, 503–508 (2007).
6. K. L. Mueller *et al*., The receptors and coding logic for bitter taste. *Nature* **434**, 225–229 (2005).
7. S. Marella *et al*., Imaging taste responses in the fly brain reveals a functional map of taste category and behavior. *Neuron* **49**, 285–295 (2006).
8. D. G. Laing, H. Panhuber, R. I. Baxter, Olfactory properties of amines and n-butanol. *Chem. Senses* **3**, 149–166 (1978).
9. M. J. Charro, E. Alcorta, Quantifying relative importance of maxillary palp information on the olfactory behavior of *Drosophila melanogaster*. *J. Comp. Physiol. A* **175**, 761–766 (1994).
10. B. Malnic, J. Hirono, T. Sato, L. B. Buck, Combinatorial receptor codes for odors. *Cell* **96**, 713–723 (1999).
11. J. L. Semmelhack, J. W. Wang, Select *Drosophila* glomeruli mediate innate olfactory attraction and aversion. *Nature* **459**, 218–223 (2009).
12. K. Yoshida *et al*., Odour concentration-dependent olfactory preference change in *C. elegans*. *Nat. Commun.* **3**, 739 (2012).
13. M. L. Guillermin, M. A. Carrillo, E. A. Hallem, A single set of interneurons drives opposite behaviors in *C. elegans*. *Curr. Biol.* **27**, 2630–2639.e6 (2017).
14. J. Kim *et al*., Rapid, biphasic CRF neuronal responses encode positive and negative valence. *Nat. Neurosci.* **22**, 576–585 (2019).
15. J. G. White, E. Southgate, J. N. Thomson, S. Brenner, The structure of the nervous system of the nematode *Caenorhabditis elegans*. *Philos. Trans. R. Soc. Lond. B Biol. Sci.* **314**, 1–340 (1986).
16. E. M. Hedgecock, R. L. Russell, Normal and mutant thermotaxis in the nematode *Caenorhabditis elegans*. *Proc. Natl. Acad. Sci. U.S.A.* **72**, 4061–4065 (1975).
17. A. Kuhara *et al*., Temperature sensing by an olfactory neuron in a circuit controlling behavior of *C. elegans*. *Science* **320**, 803–807 (2008).
18. I. Mori, Y. Ohshima, Neural regulation of thermotaxis in *Caenorhabditis elegans*. *Nature* **376**, 344–348 (1995).
19. M. Beverly, S. Anbil, P. Sengupta, Degeneracy and neuromodulation among thermosensory neurons contribute to robust thermosensory behaviors in *Caenorhabditis elegans*. *J. Neurosci.* **31**, 11718–11727 (2011).
20. L. Luo *et al*., Bidirectional thermotaxis in *Caenorhabditis elegans* is mediated by distinct sensorimotor strategies driven by the AFD thermosensory neurons. *Proc. Natl. Acad. Sci. U.S.A.* **111**, 2776–2781 (2014).
21. K. D. Kimura, A. Miyawaki, K. Matsumoto, I. Mori, The *C. elegans* thermosensory neuron AFD responds to warming. *Curr. Biol.* **14**, 1291–1295 (2004).
22. D. A. Clark, D. Biron, P. Sengupta, A. D. T. Samuel, The AFD sensory neurons encode multiple functions underlying thermotactic behavior in *Caenorhabditis elegans*. *J. Neurosci.* **26**, 7444–7451 (2006).
23. D. Ramot, B. L. MacInnis, M. B. Goodman, Bidirectional temperature-sensing by a single thermosensory neuron in *C. elegans*. *Nat. Neurosci.* **11**, 908–915 (2008).
24. D. A. Clark, C. V. Gabel, H. Gabel, A. D. T. Samuel, Temporal activity patterns in thermosensory neurons of freely moving *Caenorhabditis elegans* encode spatial thermal gradients. *J. Neurosci.* **27**, 6083–6090 (2007).
25. A. Takeishi *et al*., Receptor-type guanylyl cyclases confer thermosensory responses in *C. elegans*. *Neuron* **90**, 235–244 (2016).
26. K. Kobayashi *et al*., Single-cell memory regulates a neural circuit for sensory behavior. *Cell Rep.* **14**, 11–21 (2016).
27. Y. Tsukada *et al*., Reconstruction of spatial thermal gradient encoded in thermosensory neuron AFD in *Caenorhabditis elegans*. *J. Neurosci.* **36**, 2571–2581 (2016).
28. P. D. Walden, N. J. Cowan, A novel 205-kilodalton testis-specific serine/threonine protein kinase associated with microtubules of the spermatid manchette. *Mol. Cell. Biol.* **13**, 7625–7635 (1993).
29. M. Huang, G. Gu, E. L. Ferguson, M. Chalfie, A stomatin-like protein necessary for mechanosensation in *C. elegans*. *Nature* **378**, 292–295 (1995).
30. K. G. Miller, M. D. Emerson, J. B. Rand, Goalpha and diacylglycerol kinase negatively regulate the Gqalpha pathway in *C. elegans*. *Neuron* **24**, 323–333 (1999).
31. S. Nurrish, L. Ségalat, J. M. Kaplan, Serotonin inhibition of synaptic transmission: Galpha(0) decreases the abundance of UNC-13 at release sites. *Neuron* **24**, 231–242 (1999).
32. Y. Okochi, K. D. Kimura, A. Ohta, I. Mori, Diverse regulation of sensory signaling by *C. elegans* nPKC-epsilon/eta TTX-4. *EMBO J.* **24**, 2127–2137 (2005).
33. N. Ohnishi, A. Kuhara, F. Nakamura, Y. Okochi, I. Mori, Bidirectional regulation of thermotaxis by glutamate transmissions in *Caenorhabditis elegans*. *EMBO J.* **30**, 1376–1388 (2011).
34. H. Inada *et al*., Identification of guanylyl cyclases that function in thermosensory neurons of *Caenorhabditis elegans*. *Genetics* **172**, 2239–2252 (2006).
35. J. D. Hawk *et al*., Integration of plasticity mechanisms within a single sensory neuron of *C. elegans* actuates a memory. *Neuron* **97**, 356–367.e4 (2018).
36. S. Kato *et al*., Global brain dynamics embed the motor command sequence of *Caenorhabditis elegans*. *Cell* **163**, 656–669 (2015).
37. L. Luo *et al*., Dynamic encoding of perception, memory, and movement in a *C. elegans* chemotaxis circuit. *Neuron* **82**, 1115–1128 (2014).
38. Z. Li, J. Liu, M. Zheng, X. Z. S. Xu, Encoding of both analog- and digital-like behavioral outputs by one *C. elegans* interneuron. *Cell* **159**, 751–765 (2014).
39. A. Narayan, G. Laurent, P. W. Sternberg, Transfer characteristics of a thermosensory synapse in *Caenorhabditis elegans*. *Proc. Natl. Acad. Sci. U.S.A.* **108**, 9667–9672 (2011).
40. S. Speese *et al*., UNC-31 (CAPS) is required for dense-core vesicle but not synaptic vesicle exocytosis in *Caenorhabditis elegans*. *J. Neurosci.* **27**, 6150–6162 (2007).
41. R. Y. N. Lee, E. R. Sawin, M. Chalfie, H. R. Horvitz, L. Avery, EAT-4, a homolog of a mammalian sodium-dependent inorganic phosphate cotransporter, is necessary for glutamatergic neurotransmission in *Caenorhabditis elegans*. *J. Neurosci.* **19**, 159–167 (1999).
42. N. A. Swierczek, A. C. Giles, C. H. Rankin, R. A. Kerr, High-throughput behavioral analysis in *C. elegans*. *Nat. Methods* **8**, 592–598 (2011).
43. M. Ikeda *et al*., Circuit degeneracy facilitates robustness and flexibility of navigation behavior in *C. elegans*. bioRxiv:10.1101/385468 (5 August 2018).
44. N. A. Croll, Components and patterns in the behaviour of the nematode *Caenorhabditis elegans*. *J. Zool.* **176**, 159–176 (1975).
45. D. Kim, S. Park, L. Mahadevan, J. H. Shin, The shallow turn of a worm. *J. Exp. Biol.* **214**, 1554–1559 (2011).
46. Y. Iino, K. Yoshida, Parallel use of two behavioral mechanisms for chemotaxis in *Caenorhabditis elegans*. *J. Neurosci.* **29**, 5370–5380 (2009).
47. J. T. Pierce-Shimomura, T. M. Morse, S. R. Lockery, The fundamental role of pirouettes in *Caenorhabditis elegans* chemotaxis. *J. Neurosci.* **19**, 9557–9569 (1999).
48. W. S. Ryu, A. D. T. Samuel, Thermotaxis in *Caenorhabditis elegans* analyzed by measuring responses to defined Thermal stimuli. *J. Neurosci.* **22**, 5727–5733 (2002).
49. D. A. Clark, C. V. Gabel, T. M. Lee, A. D. T. Samuel, Short-term adaptation and temporal processing in the cryophilic response of *Caenorhabditis elegans*. *J. Neurophysiol.* **97**, 1903–1910 (2007).
50. D. Ramot, B. L. MacInnis, H. C. Lee, M. B. Goodman, Thermotaxis is a robust mechanism for thermoregulation in *Caenorhabditis elegans* nematodes. *J. Neurosci.* **28**, 12546–12557 (2008).
51. S. Rengarajan, K. A. Yankura, M. L. Guillermin, W. Fung, E. A. Hallem, Feeding state sculpts a circuit for sensory valence in *Caenorhabditis elegans*. *Proc. Natl. Acad. Sci. U.S.A.* **116**, 1776–1781 (2019).
52. A. Kocabas, C. H. Shen, Z. V. Guo, S. Ramanathan, Controlling interneuron activity in *Caenorhabditis elegans* to evoke chemotactic behaviour. *Nature* **490**, 273–277 (2012).
53. H. Suzuki *et al*., Functional asymmetry in *Caenorhabditis elegans* taste neurons and its computational role in chemotaxis. *Nature* **454**, 114–117 (2008).
54. S. H. Chalasani *et al*., Dissecting a circuit for olfactory behaviour in *Caenorhabditis elegans*. *Nature* **450**, 63–70 (2007).
55. H. Kunitomo *et al*., Concentration memory-dependent synaptic plasticity of a taste circuit regulates salt concentration chemotaxis in *Caenorhabditis elegans*. *Nat. Commun.* **4**, 2210 (2013).
56. M. B. Goodman *et al*., MEC-2 regulates *C. elegans* DEG/ENaC channels needed for mechanosensation. *Nature* **415**, 1039–1042 (2002).
57. J. S. Marvin *et al*., Stability, affinity, and chromatic variants of the glutamate sensor iGluSnFR. *Nat. Methods* **15**, 936–939 (2018).
58. J. S. Marvin *et al*., A genetically encoded fluorescent sensor for in vivo imaging of GABA. *Nat. Methods* **16**, 763–770 (2019).
59. T. Patriarchi *et al*., Ultrafast neuronal imaging of dopamine dynamics with designed genetically encoded sensors. *Science* **360**, eaat4422 (2018).
60. F. Sun *et al*., A genetically encoded fluorescent sensor enables rapid and specific detection of dopamine in flies, fish, and mice. *Cell* **174**, 481–496.e19 (2018).
61. E. Svensson *et al*., General principles of neuronal co-transmission: Insights from multiple model systems. *Front. Neural Circuits* **12**, 117 (2019).
62. M. P. Nusbaum, D. M. Blitz, E. Marder, Functional consequences of neuropeptide and small-molecule co-transmission. *Nat. Rev. Neurosci.* **18**, 389–403 (2017).
63. S. J. Shabel, C. D. Proulx, J. Piriz, R. Malinow, Mood regulation. GABA/glutamate co-release controls habenula output and is modified by antidepressant treatment. *Science* **345**, 1494–1498 (2014).
64. N. X. Tritsch, J. B. Ding, B. L. Sabatini, Dopaminergic neurons inhibit striatal output through non-canonical release of GABA. *Nature* **490**, 262–266 (2012).
65. F. Tecuapetla *et al*., Glutamatergic signaling by mesolimbic dopamine neurons in the nucleus accumbens. *J. Neurosci.* **30**, 7105–7110 (2010).
66. J. W. Muschamp *et al*., Hypocretin (orexin) facilitates reward by attenuating the antireward effects of its cotransmitter dynorphin in ventral tegmental area. *Proc. Natl. Acad. Sci. U.S.A.* **111**, E1648–E1655 (2014).
67. F. S. Vilim, E. C. Cropper, D. A. Price, I. Kupfermann, K. R. Weiss, Peptide cotransmitter release from motorneuron B16 in *Aplysia californica*: Costorage, corelease, and functional implications. *J. Neurosci.* **20**, 2036–2042 (2000).
68. F. S. Vilim, D. A. Price, W. Lesser, I. Kupfermann, K. R. Weiss, Costorage and corelease of modulatory peptide cotransmitters with partially antagonistic actions on the accessory radula closer muscle of Aplysia californica. *J. Neurosci.* **16**, 8092–8104 (1996).
69. T. Nagai, S. Yamada, T. Tominaga, M. Ichikawa, A. Miyawaki, Expanded dynamic range of fluorescent indicators for $Ca^{(2+)}$ by circularly permuted yellow fluorescent proteins. *Proc. Natl. Acad. Sci. U.S.A.* **101**, 10554–10559 (2004).
70. L. Madisen *et al*., Transgenic mice for intersectional targeting of neural sensors and effectors with high specificity and performance. *Neuron* **85**, 942–958 (2015).
71. H. Ito, H. Inada, I. Mori, Quantitative analysis of thermotaxis in the nematode *Caenorhabditis elegans*. *J. Neurosci. Methods* **154**, 45–52 (2006).